

Robust Thermal Management of Electric Vehicles Using Model Predictive Control With Adaptive Optimization Horizon and Location-Dependent Constraint Handling Strategies

Qiuha Hu^{ID}, Mohammad Reza Amini^{ID}, Ashley Wiese, Ronald Semel, Julia Buckland Seeds, Ilya Kolmanovsky^{ID}, *Fellow, IEEE*, and Jing Sun^{ID}, *Fellow, IEEE*

Abstract—The thermal management system (TMS) in electric vehicles (EVs) consumes a considerable amount of energy for maintaining the battery and cabin temperatures within the desired range. This energy consumption can significantly impact the vehicle's driving range. In this article, a model predictive control (MPC) is applied to minimize the energy consumption of the TMS while enforcing power and thermal constraints. The MPC-based thermal management strategy relies on a control-oriented model that captures the dynamics of the powertrain and thermal subsystems of an EV, as well as the coupling between these subsystems at different timescales. The relatively slow dynamics of the thermal systems call for a long prediction horizon to achieve the best performance. However, large uncertainties associated with speed prediction and preview information significantly impact the performance and robustness. In this study, an extensive sensitivity analysis is conducted to: 1) determine the key traffic and speed features over a long prediction horizon with a significant influence on the EV optimal performance and 2) study the impact of uncertainties associated with predicting these key traffic and speed features on EV performance in terms of energy efficiency and constraint enforcement. The MPC-based thermal management strategy is evaluated using real-world traffic data. To improve the robustness of the algorithm in the presence of uncertainties, a location-dependent constraint is proposed and integrated into the MPC-based thermal management strategy. The simulation results demonstrate that the location-dependent constraint enhances the capacity to enforce the battery temperature constraint, resulting in improved algorithmic robustness against uncertainties in preview information.

Index Terms—Electrical vehicles (EVs), model predictive control (MPC), power and thermal management.

Manuscript received 7 October 2022; revised 5 May 2023; accepted 19 May 2023. Date of publication 19 July 2023; date of current version 18 August 2023. Recommended by Associate Editor M. Mammarella. (*Corresponding author: Mohammad Reza Amini.*)

Qiuha Hu and Jing Sun are with the Department of Naval Architecture and Marine Engineering, University of Michigan at Ann Arbor, Ann Arbor, MI 48109 USA (e-mail: qhhu@umich.edu; jingsun@umich.edu).

Mohammad Reza Amini, Ashley Wiese, Ronald Semel, and Julia Buckland Seeds are with Ford Motor Company, Dearborn, MI 48121 USA (e-mail: mamini4@ford.com; awiese@ford.com; rsemel@ford.com; jbuckland@ford.com).

Ilya Kolmanovsky is with the Department of Aerospace Engineering, University of Michigan at Ann Arbor, Ann Arbor, MI 48109 USA (e-mail: ilya@umich.edu).

Color versions of one or more figures in this article are available at <https://doi.org/10.1109/TCST.2023.3291561>.

Digital Object Identifier 10.1109/TCST.2023.3291561

NOMENCLATURE

A_f	Frontal area of the vehicle, (m ²).
C_{bat}	Battery capacity, (Wh).
F_a	aerodynamic resistance force, (N).
F_r	Rolling resistance force, (N).
I_{bat}	Battery current, (A).
J_{bat}	Energy consumption for battery cooling, (kJ).
J_{cab}	Energy consumption for cabin cooling, (kJ).
J_{total}	Energy consumption for thermal management, (kJ).
m	Vehicle mass, (kg/s).
m_{bat}	Battery thermal mass, (g).
\dot{m}_{bat}	Mass flow rate through the battery loop, (g/s).
\dot{m}_{cab}	Mass flow rate through the cabin loop, (g/s).
\dot{m}_{cab}	Mass flow rate through the cabin loop, (g/s).
\dot{m}_{com}	Mass flow rate through the combined loops, (g/s).
P_{bat}	Battery power, (W).
P_{thm}	Power consumed for thermal management, (W).
\dot{Q}_{amb}	heat dissipated rate to the ambient, (W).
\dot{Q}_{bat}	Battery cooling power, (W).
\dot{Q}_{cab}	Cabin cooling power, (W).
\dot{Q}_{cov}	heat transfer rate of air convection, (W).
\dot{Q}_{gen}	Battery heat generation, (W).
\dot{Q}_{met}	heat transfer rate of human metabolic, (W).
\dot{Q}_{sun}	heat transfer rate of sun radiation, (W).
\dot{Q}_{ven}	heat transfer rate of ventilation, (W).
R_{bat}	Battery internal resistance, (Ω).
r	Split ratio of the coolant, (–).
T_{bat}	Battery temperature, ($^{\circ}$ C).
T_{cab}	Cabin temperature, ($^{\circ}$ C).
T_{cl}	Coolant temperature, ($^{\circ}$ C).
U_{oc}	Battery open circuit voltage, (V).
T_p	Prediction horizon length, (sec).
V_{veh}	Vehicle speed, (m/s).
ϵ	Slack variable, ($^{\circ}$ C).

ACRONYMS

CV	Constraint Violation.
COP	Coefficient of performance.
DP	Dynamic programming.
EV	Electric vehicle.

HVAC	Ventilation and air conditioning.
MPC	Model predictive control.
NEDC	New European driving cycle.
OHE	Out heat exchanger.
PMP	Pontryagin's maximum principle.
TMS	Thermal management system.
UDDS	Urban Dynamometer Driving Schedule.

I. INTRODUCTION

ELECTRIC vehicles (EVs) have attracted intensive attention in recent years. While the development of new battery technologies and favorable government policies has extended light-duty vehicle electrification, there are still issues impeding the customer acceptance of EVs. Among them, driving range anxiety has been identified as a major concern due to the relatively long time required for charging and the lagging infrastructure for fast charging [1]. Considering the significant impact thermal management has on both battery efficiency and driver/passenger comfort, improving thermal management for EVs is important, particularly in extreme weather conditions.

The EV TMS includes heating/cooling, ventilation, and air conditioning systems that maintain components onboard in their desired and safe thermal states. Cabin and battery temperature regulation are crucial for EVs, as the battery is subject to performance degradation or lifespan reduction when operating at extremely high or low temperatures, while over/under heating and cooling of the cabin may impact passengers' comfort. On the other hand, many recent studies have demonstrated the driving range reduction due to the use of TMS systems [2], [3], [4], [5]. For example, the study in [2] shows that the driving range reduction of Nissan Leaf over NEDC can be up to 9% and 22% under cooling and heating scenarios, respectively, due to the operation of the TMS system. According to the test conducted at Argonne National Laboratory, Lemont, IL, USA [6], the using of an HVAC system can reduce the driving range up to 59%.

Many recent works have addressed thermal management in EVs [7], [8], [9], [10], [11], [12], [13], [14], [15], [16], [17]. Among those, various optimization-based approaches have been developed to improve TMS efficiency and other performance attribute. DP is exploited to find the global optimal solution to the TMS [7], [8], [9]. In [7], DP was used to optimize the operation of the HVAC system on a given trip, and the improvement of cabin comfort with minimal impact on energy consumption was demonstrated. DP was also used in [8] to optimize the battery thermal management performance. PMP was used in [10] and [11] to minimize energy consumption while maintaining battery temperature within a desired range. Moreover, convex/nonlinear programming was used in [12], [13], [14], [15], [16], and [17] to enhance the performance of the electric powertrain. For instance, in [12], a framework combining high-level convex programming with low-level mixed-integer optimization was developed to maximize the driving range of an electric race car. A relationship between battery temperature and internal resistance was considered, and during the charging phases, a terminal condition of battery temperature was imposed to avoid overheating.

Furthermore, a genetic algorithm was used in [18] for cabin thermal management and achieved improved cabin comfort and driving range. Despite the reported benefits, most of the existing optimization-based approaches were conducted offline while assuming the vehicle speed, and power/thermal loads over the entire driving cycle are known a priori.

Extending existing offline optimization-based TMS to real-time presents two main challenges. First, thermal systems typically exhibit slow dynamics, necessitating a long-range prediction horizon for optimal performance. However, this can significantly increase the computational footprint, as demonstrated in prior research [19], [20], [21], [22]. For example, in [19], the prediction horizon of the MPC-based cabin thermal management is 10 min. In [20], the simulation result shows that increasing the prediction horizon from 30 sec to 180 sec resulted in reduced energy consumption for battery cooling and CV of battery temperature. However, when the prediction horizon was extended to 180 sec, the average computational time required to solve the optimization problem became unaffordable for real-time implementation. Therefore, to achieve a balanced solution between thermal management performance and computational footprint, it is crucial to understand the necessary window and key information of preview information for effective TMS implementation.

The second challenge in extending optimization-based TMS to real time is the uncertainty associated with the preview information over long-range prediction horizons, which can negatively impact optimal performance. To handle these uncertainties, various stochastic or deterministic approaches have been developed. For example, in [23], [24], and [25], a stochastic MPC was developed for real-time battery thermal management, which utilized a Markov chain representation of future vehicle speed and acceleration inferred from data from standard driving cycles. Although energy efficiency improvements were observed compared with alternative frozen-in-time predictions of vehicle speed and acceleration, the possible scenario number increased exponentially with the prediction horizon, leading to a large computational load. Therefore, the prediction horizon length adopted in [23] was only 3s. However, given the slow dynamics of thermal systems, longer horizons could potentially offer more significant improvements. In contrast, [21] developed a deterministic hierarchical MPC with piloting and scheduling layers for robust battery thermal management, assuming that the short piloting layer had access to more accurate preview information. To improve robustness, the constraints in the scheduling layer were tightened once a deviation was detected between the planned and tracked battery temperature over a short horizon. However, this approach can only detect prediction errors in the short-range horizon. Due to the slow dynamics of thermal systems, there may not be enough leading time to completely prevent CVs. A method that leverages long-term statistical information to enhance the robustness of optimal TMS for EVs is absent from the literature.

To handle the aforementioned two challenges, an MPC-based TMS framework is developed in this article to handle both battery and cabin temperatures by: 1) determining the key traffic preview information required over the prediction

horizon; 2) evaluating the impact of preview uncertainties on the optimal TMS performance; and 3) further improving the robustness of the MPC-based thermal management algorithm in the presence of inevitable uncertainties associated with long-term traffic/vehicle speed predictions.

The main contributions of this article are fourfold. First, we investigate the sensitivity of the MPC results to different prediction horizons and identify the necessary horizon length for optimal performance. Second, we propose an adaptive strategy to adjust the prediction horizon length based on the prediction of key speed features and reduce the average computational footprint. Third, we study the impact of uncertainty on MPC-based TMS performance in terms of energy efficiency and thermal CVs. Finally, we demonstrate a location-dependent constraint handling strategy that leverages real-world historical data to balance the tradeoff between energy efficiency and mitigating thermal CVs.

This article is organized as follows. The power and thermal models of the electrical vehicle adopted in this article are introduced in Section II. Section III presents the MPC results with different prediction horizons and identifies the key speed/traffic features. Then, the impact of uncertainties in the speed predictions on the optimal TMS performance is quantified in Section IV. Finally, in Section V, the developed MPC-based thermal management strategy is evaluated using real-world traffic data, and a location-dependent constraint handling strategy is proposed to improve the robustness of the algorithm against the uncertainties in speed preview.

II. POWERTRAIN AND THERMAL MODELS OF AN ELECTRICAL VEHICLE

A. Vehicle Traction Power Model

The vehicle traction power (P_{trc}) is determined by

$$P_{trc} = V_{veh}(m\dot{V}_{veh} + F_r + F_a) \quad (1)$$

where F_r and F_a represent the rolling and aerodynamic resistance force, respectively, which are calculated as follows:

$$F_r = C_r mg \quad (2)$$

$$F_a = 0.5\rho A_f C_d V_{veh}^2 \quad (3)$$

where C_r and C_d are the coefficient of rolling and aerodynamic resistance, A_f is the frontal area of the vehicle, and ρ is the air density. The vehicle is assumed to be on a flat road and the effects of road grade and wind are not considered. As the proposed strategy in what follows is strongly based on vehicle traction power preview, these additional dependencies can be easily included in (2).

B. Integrated Thermal Management System

Fig. 1 depicts a schematic of the integrated TMS of an EV, which consists of the refrigerant loop, as well as cabin and battery cooling loops. The refrigerant absorbs heat from the battery and cabin coolant, while the OHE dissipates the absorbed heat to the ambient and provides cold coolant. This assumption is based on the premise that the lower level controller/actuators can effectively maintain the coolant

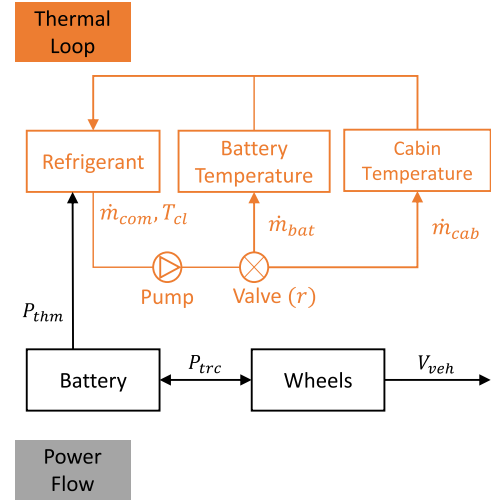


Fig. 1. Schematic of integrated TMS of an EV.

temperature and the coolant dynamics are negligible compared with the battery and cabin thermal dynamics. Note that the outlet coolant temperature (T_{cl}) of the refrigerant system is assumed to be constant. The battery and cabin coolant is circulated by an electric pump through the combined cabin and battery loops. Its mass flow rate is denoted by \dot{m}_{com} . The coolant splits into battery and cabin cooling loops by a three-way valve with a mass flow rate of \dot{m}_{bat} and \dot{m}_{cab} , respectively. The coolant flow rates follow the mass conservative law

$$\dot{m}_{com} = \dot{m}_{bat} + \dot{m}_{cab} \quad (4)$$

$$\dot{m}_{cab} = r\dot{m}_{com} \quad (5)$$

$$\dot{m}_{bat} = (1 - r)\dot{m}_{com} \quad (6)$$

where r is the split ratio of the coolant, which is controlled by the three-way valve. The cold coolant provides the cooling power to the battery (\dot{Q}_{bat}) and cabin (\dot{Q}_{cab}) through their heat exchanges. The cooling power of each loop is determined by the following equations:

$$\dot{Q}_{bat} = \alpha(\dot{m}_{bat})(T_{bat} - T_{cl}) \quad (7)$$

$$\dot{Q}_{cab} = \beta(\dot{m}_{cab})(T_{cab} - T_{cl}) \quad (8)$$

where α and β are the heat exchange coefficients, which increase as the coolant flow rate increases. Equations (7) and (8) are based on Newton's law of cooling, and the coefficients of heat exchange are functions of coolant rate, which is assumed to be linear in this study. The linear relationship is used for simplicity, and we do not have enough data to provide a more accurate relationship between cooling power and coolant flow rate. On the other hand, the focus of this study is to develop the optimal control framework, and the developed framework can be easily extended with more accurate models. The cabin and battery cooling power can be controlled by the electric pump and three-way valve. The former adjusts \dot{m}_{com} and the latter changes r .

The power consumption of the TMS (P_{thm}) is calculated as follows:

$$P_{thm} = \frac{\dot{Q}_{bat} + \dot{Q}_{cab}}{COP} \quad (9)$$

where COP is the coefficient of performance describing the efficiency of the TMS, and P_{sys} includes the power consumed for the compressor and electric pump. The representation of COP, as a function of the cooling power, is adopted from [26] and corresponds to R-134a coolant. Based on this model COP decreases as the total cooling power increases.

C. Battery Thermal Submodel

The battery current (I_{bat}) are represented using an equivalent circuit model

$$I_{\text{bat}} = \frac{U_{\text{oc}} - \sqrt{U_{\text{oc}}^2 - 4R_{\text{int}}P_{\text{bat}}}}{2R_{\text{int}}} \quad (10)$$

where R_{int} and U_{oc} are internal resistance and open-circuit voltage, respectively. The variable P_{bat} is the total power demanded by the battery, including the power consumed for vehicle traction (P_{trc}) and by TMS (P_{thm}).

The battery heat generation is mainly attributed to the internal resistance and is given by

$$\dot{Q}_{\text{gen}} = I_{\text{bat}}^2 R_{\text{int}}. \quad (11)$$

The battery is modeled as a lumped mass and the dynamic of temperature, T_{bat} , are expressed as

$$\dot{T}_{\text{bat}} = f_{\text{bat}}(t) = \frac{1}{m_{\text{bat}}C_{\text{bat}}}(\dot{Q}_{\text{gen}} + \dot{Q}_{\text{amb}} - \dot{Q}_{\text{bat}}) \quad (12)$$

where m_{bat} and C_{bat} are the thermal mass and specific heat capacity of the battery, respectively, and \dot{Q}_{amb} is the rate of the heat dissipated to the ambient by air convection, which is proportional to the temperature difference between battery and ambient.

D. Cabin Thermal Submodel

The cabin is also modeled as a lumped mass so that the cabin temperature dynamics are expressed as

$$\begin{aligned} \dot{T}_{\text{cab}} &= f_{\text{cab}}(t) \\ &= \frac{1}{m_{\text{cab}}C_{\text{cab}}}(\dot{Q}_{\text{sun}} + \dot{Q}_{\text{cov}} + \dot{Q}_{\text{ven}} + \dot{Q}_{\text{met}} - \dot{Q}_{\text{cab}}) \end{aligned} \quad (13)$$

where m_{cab} and C_{cab} are the thermal mass and specific heat capacity of the cabin, respectively. \dot{Q}_{sun} , \dot{Q}_{cov} , \dot{Q}_{ven} , and \dot{Q}_{met} are the heat transfer rate of sun radiation, air convection, air ventilation, and human metabolic activities, respectively. The detailed formulation of each heat source term in (13) can be found in [27].

III. MPC-BASED THERMAL MANAGEMENT OF AN EV

A. MPC Formulation for TMS

We consider EV operating with hot ambient temperatures (38 °C). To reduce the energy consumption by TMS and enforce the constraints on thermal states and control inputs, our MPC approach is based on the following discrete-time

finite horizon optimal control problem

$$\begin{aligned} \min_{\dot{m}_{\text{com}}(i), r(i)} \quad & \sum_{i=t}^{t+N-1} \{(\dot{Q}_{\text{cab}}(i) + \dot{Q}_{\text{bat}}(i))/\text{COP} + a_1\epsilon_1^2 + a_2\epsilon_2^2 \\ & + b_1\Delta\dot{m}_{\text{com}}(i) + b_2\Delta r(i)\} \\ \text{s.t.} \quad & T_{\text{bat}}(i+1) = T_{\text{bat}}(i) + f_{\text{bat}}(i)\Delta t \\ & T_{\text{cab}}(i+1) = T_{\text{cab}}(i) + f_{\text{cab}}(i)\Delta t \\ & \dot{Q}_{\text{bat}}(i) = \alpha(\dot{m}_{\text{bat}}(i))(T_{\text{bat}}(i) - T_{\text{cl,out}}) \\ & \dot{Q}_{\text{cab}}(i) = \beta(\dot{m}_{\text{cab}}(i))(T_{\text{cab}}(i) - T_{\text{cl,out}}) \\ & 24 \text{ }^\circ\text{C} \leq T_{\text{cab}}(i) \leq 25 \text{ }^\circ\text{C} + \epsilon_1 \\ & 15 \text{ }^\circ\text{C} \leq T_{\text{bat}}(i) \leq 35 \text{ }^\circ\text{C} + \epsilon_2 \\ & 0 \leq \dot{m}_{\text{com}}(i) \leq \dot{m}_{\text{max}} \\ & 0 \leq r(i) \leq 1 \\ & 0 \leq \epsilon_{1,2}(i) \leq 5 \text{ }^\circ\text{C} \\ & \Delta\dot{m}_{\text{com,min}} \leq \Delta\dot{m}_{\text{com}}(i) \leq \Delta\dot{m}_{\text{com,max}} \\ & \Delta r_{\text{min}} \leq \Delta r(i) \leq \Delta r_{\text{max}} \end{aligned} \quad (14)$$

where f_{bat} and f_{cab} are defined in (12) and (13), respectively. Δt is the sampling time, and $T_p = N\Delta t$ is the prediction horizon length. The cost function in (14) consists of three terms: 1) the power consumption for cabin and battery cooling; 2) penalty on slack variables, ϵ_1 and ϵ_2 , which relax T_{cab} and T_{bat} upper bounds; and 3) penalty terms for the rate of change of control variables, \dot{m}_{com} and r . Note that the optimization problem (14) is nonlinear mainly because of (10) and (11).

Remark 1: The rate of change of flow ($\Delta\dot{m}_{\text{com}}$) and the split (Δr) are constrained and penalized in (14) because the rapid change of cabin cooling power could be perceived unfavorably to passengers' comfort.

Remark 2: The lower and upper bounds on T_{cab} are set as 24 °C and 25 °C, respectively, assuming that the cabin temperature setpoint is set to 24.5 °C with an allowable deviation of 0.5 °C. The desired operating temperature range for the battery is from 15 °C to 35 °C, consistent with [28]. The upper bounds of both cabin and battery temperature are treated as soft constraints, using the slack variables, ϵ_1 and ϵ_2 , in the cost function. The maximum values of ϵ_1 and ϵ_2 are both 5 °C.

Remark 3: The parameters in the cost function of (14) are selected based on the following considerations. First, the penalty weights b_1 and b_2 are set large enough ($b_1 = b_2 = 5 \cdot 10^4$) to make sure there are no significant oscillations of the \dot{m}_{com} and r . Second, a_1 and a_2 determine the strictness of the upper bound constraints of battery and cabin temperature. In this study, we prioritize the cabin temperature constraints, and therefore, $a_1 = 10^6$ and $a_2 = 10^4$, to reliably maintain cabin temperature within the desired range over the entire trip.

Note that the upper limits of cabin and battery temperature are soft and slack variables have been added to avoid the infeasibility of optimization problems. The MPC feedback law is informed by the first element of the optimal control sequence. The subsequent simulations are performed on a desktop computer with an Intel i7-10750H @ 2.60-GHz processor. The optimization problem (14) is solved using MPCTools [29] in MATLAB. It uses the Interior Point OPTimizer (IPOPT) [30]

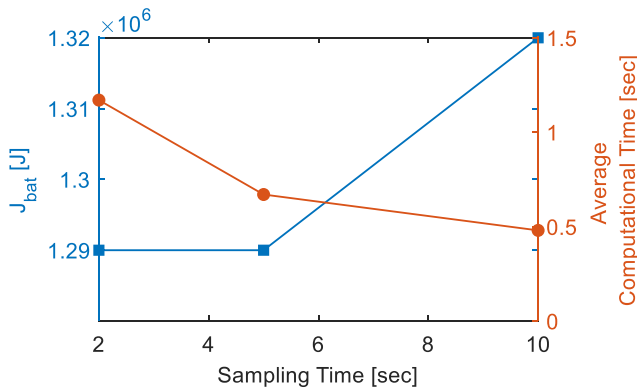


Fig. 2. Energy consumption for battery cooling (J_{bat}) and average computational time results of Case II with different sampling times.

from CasADi package [31] for solving the nonlinear programming problem. In the simulations, the initial cabin temperature is chosen as 25 °C and the initial battery temperature as 34 °C. Note that these initial values fall within the ranges allowed by the constraints, and the cool-down phase is not considered in this study.

B. Impact of Prediction Horizon Length on MPC-Based TMS Performance

The relatively slow dynamics of thermal systems call for a long prediction horizon for MPC to achieve the best performance [21]. In this study, to investigate the impact of the prediction horizon length on energy consumption and constraint enforcement, two cases with different prediction horizon lengths are defined as follows.

- 1) *Case I*: Prediction horizon length (T_p) is 50 sec, and $T_{bat,max} = 35$ °C.
- 2) *Case II*: Prediction horizon length (T_p) is 200 sec, and $T_{bat,max} = 35$ °C.

Note that in this section, it is assumed that accurate vehicle speed information over the prediction horizon is known a priori, regardless of the length of the prediction horizon. This assumption will be relaxed in the later sections when investigating the impact of uncertainties.

Remark 4: For both two cases, the sampling time, Δt , in (14) is chosen to be 5 sec. A sensitivity analysis on the sampling time was conducted, and the simulation results of Case II with different sampling times are presented in Fig. 2. The value of 5 sec is chosen as it provides the best tradeoff between energy efficiency and computational footprint.

The simulated driving cycle combines the Environmental Protection Agency (EPA) UDDS with Highway Fuel Economy Test Cycle (HWFET), which includes both city and highway driving scenarios. Fig. 3 summarizes the simulation results. As one can see, over the entire trip, T_{cab} can be maintained in the comfort range for both Cases I and II, while multiple violations of T_{bat} can be observed for Case I when the prediction horizon is 50 sec. As highlighted in Fig. 3, such violations happen when a large current is generated as the vehicle is undergoing aggressive acceleration or deceleration maneuvers. This CV, if occurs often enough, may negatively impact the battery state-of-health and longevity [28]. It can be also seen from Fig. 3(e) that \dot{m}_{com} approaches its limit over

TABLE I

ENERGY CONSUMPTION AND COMPUTATIONAL TIME RESULTS FOR CASES I, I*, II, AND III. J_{bat} AND J_{cab} ARE THE ENERGY CONSUMPTION FOR THE BATTERY AND CABIN TMS. J_{total} IS THE TOTAL ENERGY CONSUMPTION FOR TMS

Case	I	I*	II	III
J_{bat} [kJ]	1339	1465	1315	1317
J_{cab} [kJ]	4477	4526	4459	4460
J_{total} [kJ]	5817	5992	5774	5777
Computational Time (Average) [sec]	0.20	0.21	0.53	0.26

the highlighted time periods for Case I. For Case II with a long prediction horizon (200 sec), MPC has more awareness of the large traction power in the near future, and thus, the controller cools down T_{bat} in advance to prevent the CV.

Intuitively, one simple approach to enforce the T_{bat} constraint in Case I is to tighten the upper bound of the soft constraint, $T_{bat,max}$, based on which a modified version of Case I, Case I* is defined as follows.

- 1) *Case I**: Prediction horizon length (T_p) is 50 sec, and $T_{bat,max} = 33$ °C.

Note that $T_{bat,max}$ is reduced by 2 °C in Case I* according to the maximum CV observed in Fig. 3(d), while no constraint tightening is applied to Case II. Fig. 4 presents the simulation results of Case I*. It can be observed that by tightening the upper bound of the soft constraint, T_{bat} constraint can be successfully enforced over the entire trip for Case I*. However, the conservative approach leads to extra energy consumption for the TMS, as shown in Table I. It can be seen that compared with Case I, Case I* consumes 9.4% and 1.1% more energy for battery (J_{bat}) and cabin (J_{cab}) cooling, respectively. Moreover, Case II achieves the best energy efficiency among all three cases with good enforcement of thermal constraints over the entire trip, thanks to the long-range prediction horizon. The above-mentioned analyses demonstrate that for the MPC-based thermal management for an EV, a longer prediction horizon allows a less conservative strategy to enforce the thermal constraints while providing better energy efficiency for this use case.

C. Key Features in the Speed Preview

It can be seen from Fig. 3(d) that the optimal T_{bat} trajectories are considerably different for different prediction horizons only when there is a large change in traction power. If there is no such event, e.g., from $t = 500$ to 1500 sec, Case I and II exhibit similar results for T_{bat} , and extending the prediction horizon does not improve energy efficiency and constraint enforcement. This case study identifies the large traction power associated with aggressive acceleration and deceleration maneuvers as one of the key events that significantly impact performance, and therefore, should be captured in the speed preview.

Fig. 5 demonstrates a key event caused by large traction power. The heat generation is calculated using (1), (10), and (11), while the maximum battery cooling power ($\dot{Q}_{bat,max}$) is calculated based on (8) and (9). It is important to note that due

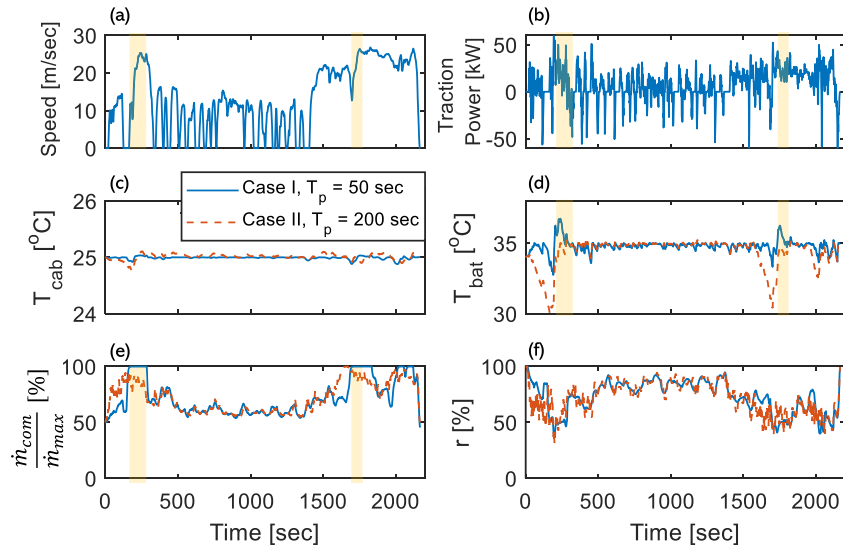


Fig. 3. MPC results with different prediction horizons based on Cases I and II. (a) Vehicle speed profile. (b) Traction power profile. (c) Cabin temperature. (d) Battery temperature. (e) Normalized coolant flow rate. (f) Coolant split ratio.

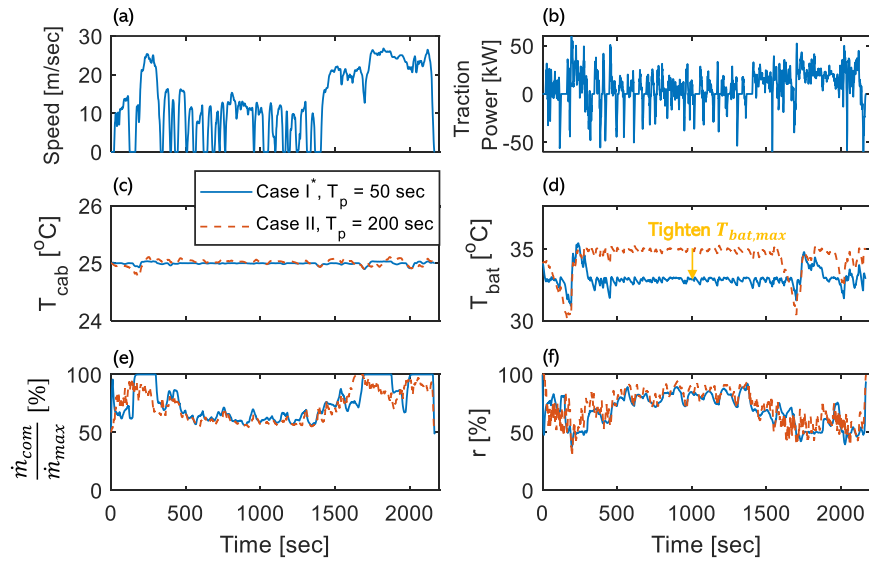


Fig. 4. MPC results with different prediction horizons based on Cases I* and II. (a) Vehicle speed profile. (b) Traction power profile. (c) Cabin temperature. (d) Battery temperature. (e) Normalized coolant flow rate. (f) Coolant split ratio.

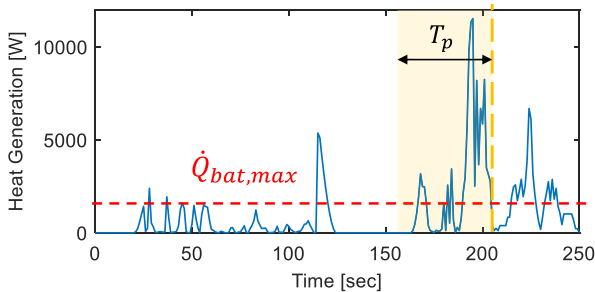


Fig. 5. Identify the key event over the prediction horizon based on the heat generation profile.

to the coupling of the cabin and battery cooling system, the $\dot{Q}_{bat,max}$ is also determined by the cabin cooling power (\dot{Q}_{cab}). For this study, the cabin thermal management is prioritized, and \dot{Q}_{cab} is set to ensure the cabin temperature remains within the desired range throughout the trip. As shown in Fig. 5, there are time periods where the battery heat generation exceeds

the maximum battery cooling power ($\dot{Q}_{bat,max}$), leading to the violation of the battery temperature constraint. To avoid this violation, battery precooling is necessary, which requires the controller to detect events in advance. Additionally, the total delivered cooling power must be greater than the generated heat, as described by the following inequality equation:

$$\sum_{i=t}^{t+N-1} \dot{Q}_{bat,max}(i) \Delta t \geq \sum_{i=t}^{t+N-1} H_{gen}(i) \Delta t \quad (15)$$

where H_{gen} denotes the battery's heat generation rate. Note that the prediction horizon length is given by $N\Delta t = T_p$, where N is the number of time steps, Δt is the sampling time, and T_p is the length of the horizon. If the inequality given by (15) cannot be satisfied over a short-range horizon, for instance, when $T_p = 50$ sec, it indicates that the prediction horizon is insufficient for precooling the battery. Thus, we define the event of high traction power when the inequality in (15) cannot

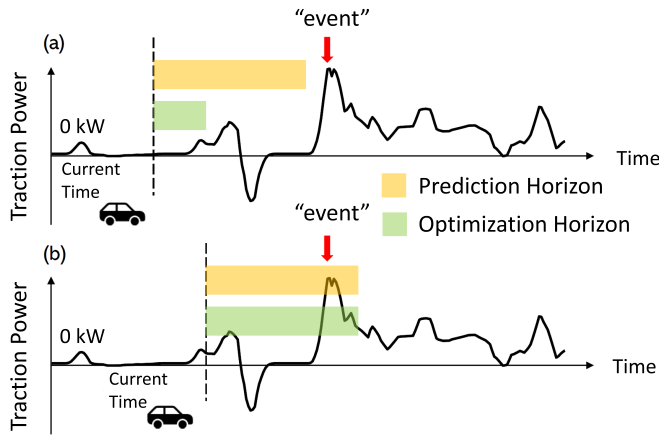


Fig. 6. Concept of Case III. (a) When the key “event” of large traction power is not detected over the prediction horizon, a short horizon is adopted for MPC. (b) When the key “event” is detected within the prediction horizon, a long optimization horizon is adopted.

be satisfied over a short-range horizon, and a longer range horizon is required to prevent CV.

To capture the significant events over the long prediction horizon without being overburdened with computation, we propose the concept of adaptive optimization horizon, as presented in Fig. 6. A long prediction horizon is applied to cover the key speed events, and if such event is not detected over the prediction horizon, as shown in Fig. 6(a), a short-range optimization horizon is applied to the MPC problem (14). Whereas, if the key “event” is predicted to occur within the prediction horizon, as shown in Fig. 6(b), a long optimization horizon is applied to (14). To demonstrate the impact of the adaptive prediction horizon, a new case study (Case III) with adaptive prediction horizon length is considered as follows.

- 1) *Case III*: Adaptive optimization horizon length, and $T_{\text{bat,max}} = 35^\circ\text{C}$.

In this study, the long and short prediction horizon lengths are set as 200 and 50 sec, respectively. The simulation results of Case III are presented in Fig. 7. Table I summarizes the energy consumption and computational time result of different cases. It can be seen that Cases II and III provide a similar trajectory of T_{bat} and energy consumption, which confirms that the long-range optimization horizon is only needed when the key events occur over the prediction horizon. Moreover, compared with Case II, Case III reduces the average computational time without compromising performance, which is important as other functions can be run in a shared processor due to reduced average computation time and the reduction in power consumption. Note that although the average computational time is reduced, for practical implementation, the computational time of the worst case has not been reduced by the proposed strategy.

IV. ROBUSTNESS OF MPC-BASED THERMAL MANAGEMENT AGAINST UNCERTAINTIES IN VEHICLE SPEED PREVIEW

For the analysis in Section III, an accurate speed preview over the prediction horizon is assumed, which is not

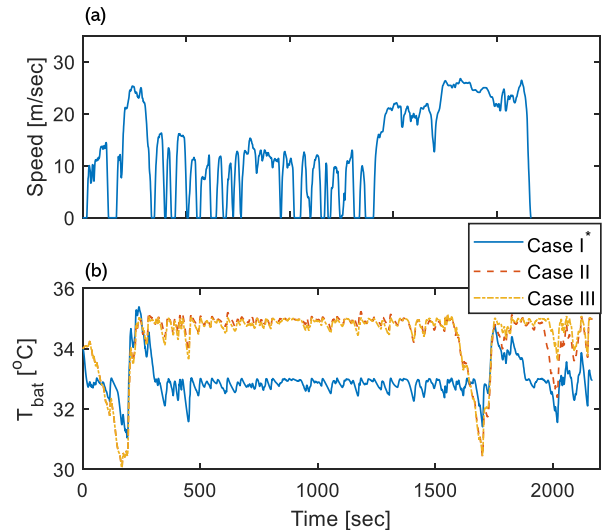


Fig. 7. MPC results of Cases I*, II, and III. (a) Vehicle speed profile. (b) Battery temperature.

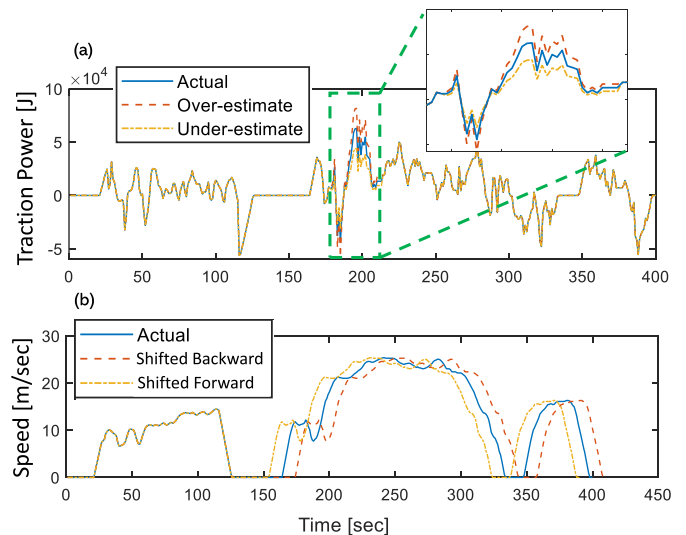


Fig. 8. Concept of two types of uncertainties. (a) Event magnitude (traction power) is overestimated or underestimated. (b) Event timing is shifted backward and forward.

realistic, particularly when the prediction horizon is relatively long. In this section, we evaluate the robustness of the MPC-based TMS performance against the errors in forecasting the speed-related key events. Focusing on the impactful period of high traction power, we consider two different types of uncertainties, as shown in Fig. 8. Namely, the over- and under-estimation of the magnitude [Fig. 8(a)] and the wrong prediction of the timing [Fig. 8(b)]. As vehicle acceleration occurs after a stop, difficulties in estimating the stop time will lead to errors in predicting the time of acceleration. While both types of uncertainties are unavoidable in real applications, we consider them separately in this study.

To study the impact of the first type of uncertainty, three cases are defined as follows.

- 1) *Case A*: The preview information is accurate.
- 2) *Case B*: The traction power during the event period is 30% overestimated.

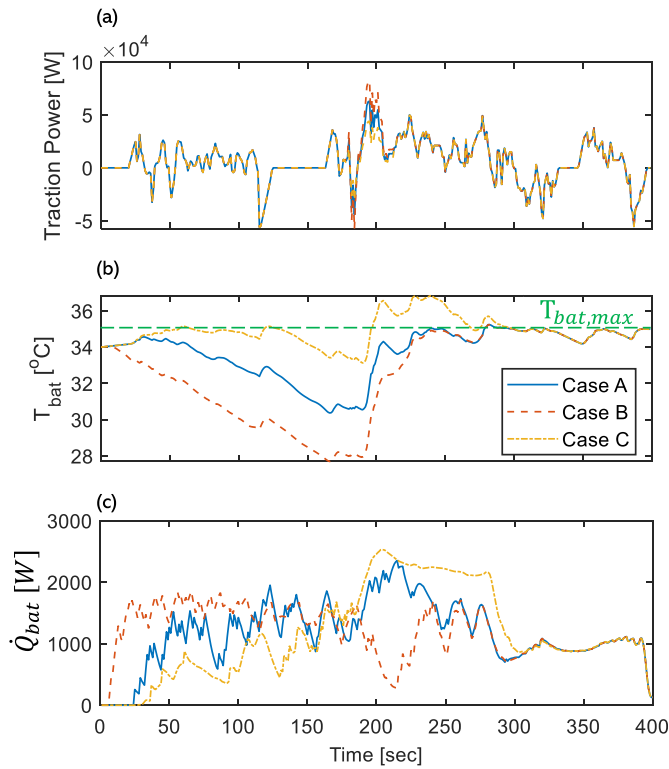


Fig. 9. MPC-based thermal management results for Cases A–C. (a) Actual and predicted traction power. (b) Battery temperature. (c) Battery cooling power.

- 3) *Case C*: The traction power during the event period is 30% underestimated.

For all three cases, the prediction horizon is set to 200 sec. The simulation results are presented in Fig. 9. With accurate preview information, T_{bat} constraint of Case A is enforced by precooling the battery before the upcoming aggressive acceleration event. Compared with Case A, in Case B, T_{bat} magnitude decreases to a lower value because the traction power is overestimated, and accordingly, more internal heat is predicted to be generated during the event period. Conversely, due to the underestimation of the traction power, in Case C, TMS does not provide enough precooling for T_{cab} , which results in the CV after the event. The energy consumption for battery cooling (J_{bat}) and accumulated CV with different levels of uncertainties are summarized in Fig. 10. Note that negative uncertainty values reflect the underestimation of the traction power while positive values reflect over-estimation. It can be seen that Case A achieves the best energy efficiency while enforcing the constraints with accurate preview information. When the traction power is overestimated, although no CV occurs, the energy consumption for battery cooling increases as the uncertainty increases. This is because of the extra thermal load imposed by the TMS on the battery to decrease T_{cab} to a lower value in the precooling phase, as shown in Fig. 9(c). On the other hand, when the traction power is underestimated, both energy consumption and the accumulated CV increase as the uncertainty increases. As shown in Fig. 9(c), because Case C does not provide enough precooling when T_{bat} exceeds $T_{bat,max}$, a larger \dot{Q}_{bat} is required to prevent a prolonged period of time with CV, which as discussed earlier,

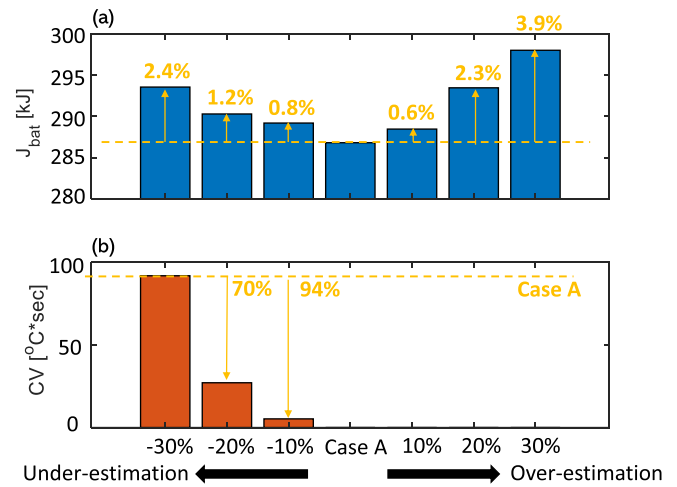


Fig. 10. Summary of the results with different levels of uncertainties in traction power magnitude estimation. (a) Energy consumed for battery cooling (J_{bat}). (b) Accumulated battery temperature CV.

reduces the efficiency (COP) of the TMS and leads to extra energy consumption.

To study the impact of the second type of uncertainty, the following three cases are considered.

- 1) *Case a*: The preview information is accurate.
- 2) *Case b*: Event timing is predicted to be 30 sec later than the actual time.
- 3) *Case c*: Event timing is predicted to be 30 sec earlier than the actual time.

The simulation results are shown in Fig. 11. It can be seen that for Case b, the controller decreases T_{bat} with a delay and does not provide enough precooling, which results in battery temperature CV. On the other hand, for Case c, T_{bat} is first decreased and then maintained at a lower value until the high traction power event occurs. Moreover, no CV is observed for Case c as Case c involves the same level of precooling as Case a with accurate preview information. The energy consumption and the accumulated temperature CV with different levels of uncertainties in event timing are summarized in Fig. 12. The negative cases represent the scenarios when the event is predicted to be earlier than the actual high traction power event, and the positive ones are those predicted to be later than the actual event. Similar to the trend shown in Fig. 10, the energy consumption increases as the uncertainty increases in either direction, and CV occurs only when the event is predicted to be later than the actual high traction power event.

Thus, the accuracy of predicting the high traction power event can significantly affect the optimal performance of MPC-based TMS. The errors in estimating the event timing and magnitude can reduce the energy efficiency of the TMS by performing over-cooling or under-cooling prior to the event. Moreover, the failure of providing enough precooling could increase CV.

V. EVALUATION OF MPC-BASED TMS PERFORMANCE USING REAL-WORLD TRAFFIC DATA

The benefits of the MPC-based thermal management for EVs were studied in Section III under the assumption that

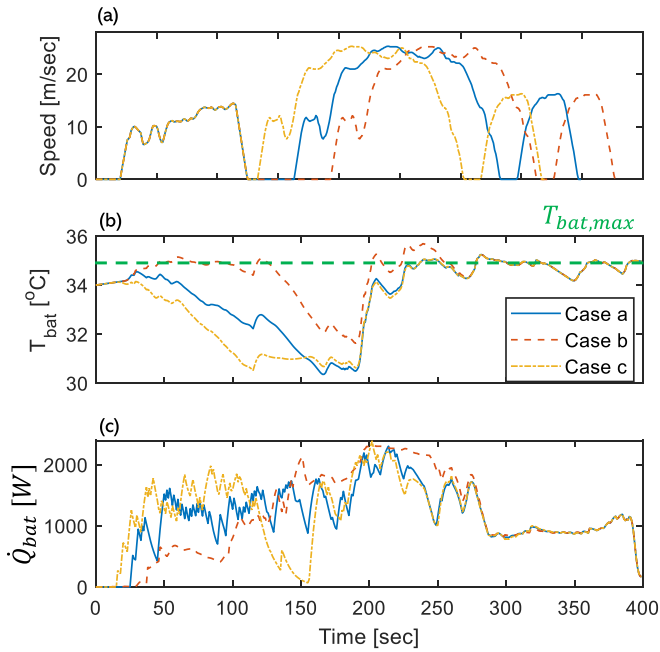


Fig. 11. MPC-based thermal management results, for Cases a–c. (a) Actual and predicted traction power. (b) Battery temperature. (c) Battery cooling power.

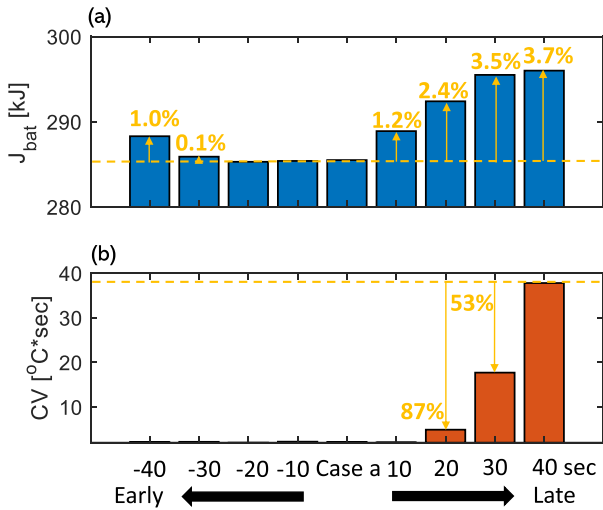


Fig. 12. Summary of the results with different levels of uncertainties in predicting the high traction power event timing. (a) Energy consumption for battery cooling (J_{bat}). (b) Accumulated CV.

the speed preview is available. The impact of uncertainties on the TMS performance was investigated in Section IV, demonstrating that the errors in predicting high traction power events will diminish the benefits of the predictive approach for TMS. In this section, the MPC performance is further evaluated using real-world traffic data. Based on insights gained in Section IV and in this section, a strategy to enhance the robustness of the MPC-based thermal management algorithm is presented.

A. MPC Results Based on Real-World Traffic Data

In this section, we apply the MPC-based thermal management strategy to the commuting driving cycle data collected from a test vehicle, which was following the same route between campus and home during commuting hours. The trips follow the exact same route with the same start and end points. Fig. 13 presents the simulation results of three different

sample trips randomly selected from the database for the same vehicle. Note that even though we assume accurate preview information over the prediction horizon, Case I, with a shorter prediction horizon, fails to enforce the T_{bat} constraint for all sample trips. The T_{bat} CVs happen at different times during the trip for different sample trips, and the severity of CVs also differs. The above-mentioned observations demonstrate that even for the repeated commuting cycle data, the aggressive acceleration events have large variations in their temporal distribution, as well as in their magnitudes from one trip to another. On the other hand, although Case II enforces the constraint over the entire trip for these three trips, it requires accurate preview information over a long prediction horizon, which may not be available in reality. Therefore, it is important to understand the impact of uncertainties associated with such real-world traffic data and improve the robustness of the MPC-based thermal management algorithm accordingly.

B. Long-Range Vehicle Speed Prediction for Implementation in MPC-Based TMS

To relax the initial assumption that the vehicle speed preview is accurate, we use vehicle speed data collected from a vehicle driving an urban route. Besides, a data-driven speed prediction framework is adopted to provide long-range speed prediction based on spatial-domain commute data. This data-driven speed prediction strategy explores the patterns in vehicle speed for recurrent trips in the spatial domain to inform speed predictions by providing an average long-range estimate of the vehicle speed.

Remark 5: In this work, we focus on commercial vehicles (e.g., delivery trucks and transit vans) that typically run fixed routes. For those vehicles, the assumptions about the known routes and the availability of historical speed data can be justified. The data used for speed prediction are collected from the same test vehicle, for which three sample trips are shown in Fig. 13. The test vehicle follows the same commuting route on workdays, allowing our analysis in Section V to assume prior knowledge of the vehicle’s route. The primary source of uncertainty in our analysis is the variation in vehicle speed over the same route. More details of the data and the data-driven speed prediction approach can be found in our previous work [32].

The aggregated vehicle speed data from around 20 trips are plotted in Fig. 14 in both the time and spatial domains. It can be observed that vehicle speed has a large variability in the time domain [Fig. 14(a)], due to the offset caused by different pass/stop events and different traffic signal timing and phasing at intersections. In contrast, the variability of the same data in the spatial domain is much smaller, suggesting a more deterministic relationship between the average vehicle speed and locations along the trip. The average vehicle speed shown in Fig. 14(b) is leveraged to provide preview information over the long horizon.

Because the MPC is solved in the time domain, the spatial vehicle speed prediction needs to be converted to the time domain by numerically integrating the following differential equation:

$$\frac{dv}{dt} = v \frac{dv}{ds}. \tag{16}$$

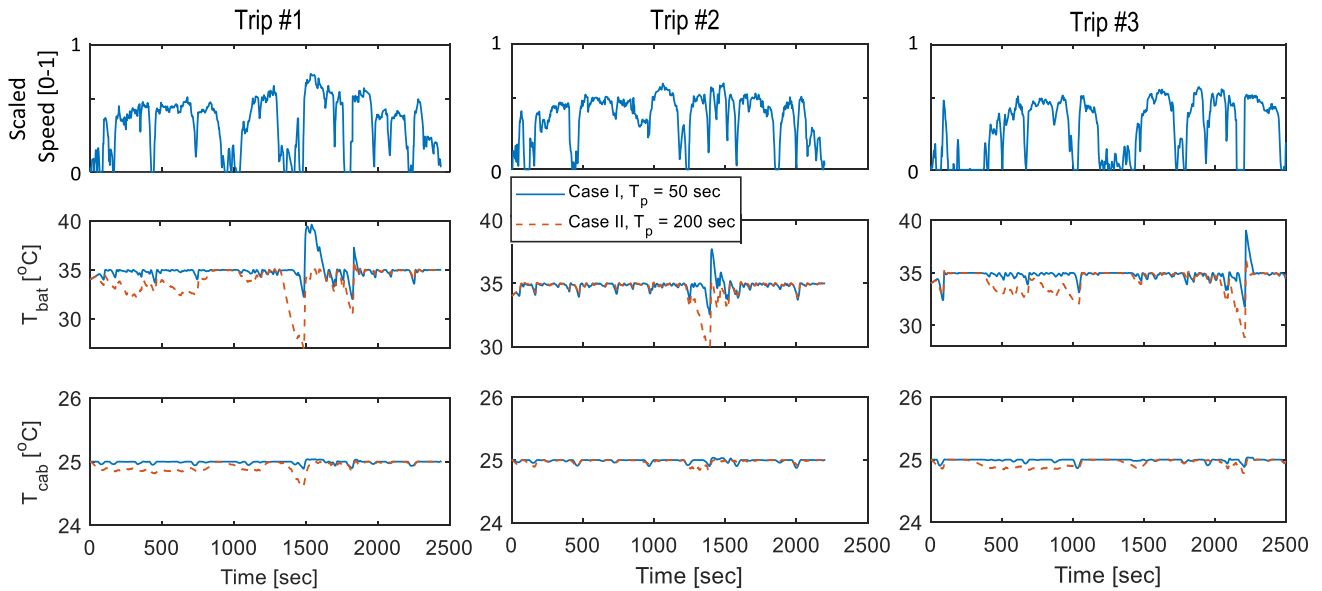


Fig. 13. MPC-based thermal management results over three sample trips from the same test vehicle driving the same route.

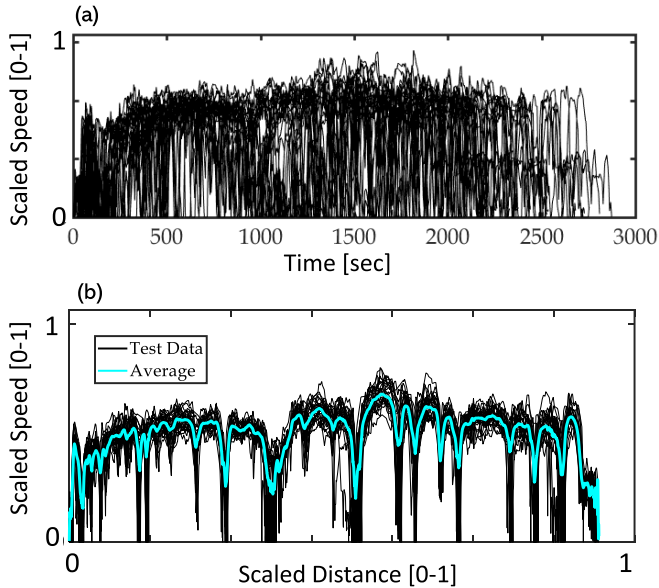


Fig. 14. Aggregated vehicle speed profiles collected from a test vehicle repeating a specific trip on an urban road: (a) in the time domain and (b) the spatial domain with the average vehicle speed of the test vehicle.

As shown in Fig. 14, while the average speed preview captures the main trends and the location of high traction power events, it is subject to uncertainties. To investigate the impact of these uncertainties associated with real-world traffic data, three cases are considered as follows.

- 1) *Case 1*: The preview information is accurate and the prediction horizon length is 50 sec; $T_{\text{bat,max}} = 30^\circ\text{C}$ over the entire trip.
- 2) *Case 2*: The preview information is accurate and the prediction horizon length is 200 sec; $T_{\text{bat,max}} = 35^\circ\text{C}$ over the entire trip.
- 3) *Case 3*: The preview information is based on the average speed shown in Fig. 14 and is subject to uncertainties.

The prediction horizon length is 200 sec; $T_{\text{bat,max}} = 35^\circ\text{C}$ over the entire trip.

Similar to Case 1* discussed in Section III-B, with a short prediction horizon, Case 1 has a tightened $T_{\text{bat,max}}$ as compared with Cases 2 and 3 to prevent CV. In this case, $T_{\text{bat,max}}$ is tightened by 5°C based on the maximum T_{bat} CV observed. Since a long prediction horizon is used in Case 2 and the preview information is assumed to be accurate, there is no need to adjust the upper bounds. For Case 3, we set $T_{\text{bat,max}} = 35^\circ\text{C}$. The state trajectories in three cases based on one sample trip from the commute data are presented in Fig. 15, and the energy consumption and accumulated CV results are summarized in Fig. 16.

It can be seen from Fig. 16 that in both Case 1 and Case 2, T_{bat} constraint is successfully enforced over the entire trip. However, to achieve this goal, compared with Case 2, Case 1 consumes 30.1% more energy for battery cooling due to a tightened constraint. Case 1 confirms that a short prediction horizon leads to a less energy efficient and more conservative TMS performance. On the other hand, while the long-range prediction horizon is applied to Case 3, T_{bat} CV still happens. This is because of the uncertainty associated with the long-range speed preview. As presented in Fig. 14(b), while the average speed inferred in the spatial domain provides an identifiable pattern for vehicle speed profiles, it is still subject to errors due to the variance in acceleration/deceleration and the offset of stop/departure time on different work days from one trip data to another. Such errors, as discussed in Section IV, could degrade the MPC-based TMS performance.

The above-mentioned analyses demonstrate the limitations of the existing MPC-based thermal management strategies in response to uncertainties in speed preview, specifically over a long range which is needed for TMS. Such limitations in the baseline MPC design call for improved robustness of the optimization algorithm without making the TMS controller design conservative. To address this limitation, a location-dependent constraint handling strategy is proposed in Section V-C.

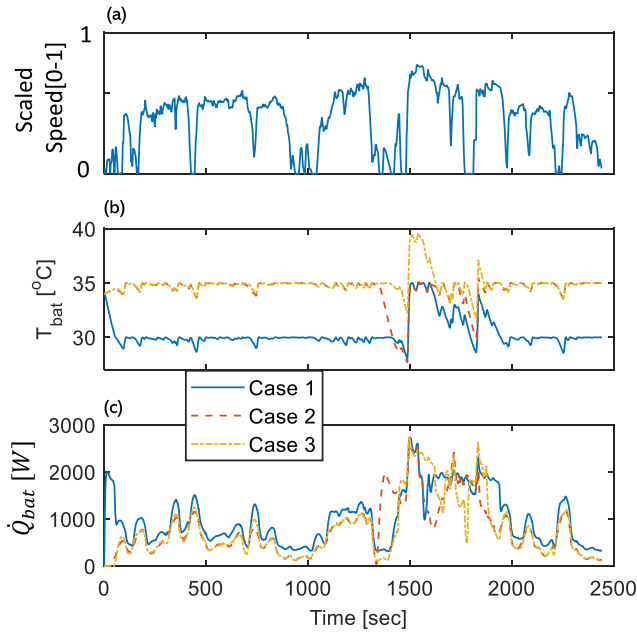


Fig. 15. State trajectories of Cases 1–3. (a) Scaled vehicle speed. (b) Battery temperature. (c) Battery cooling power.

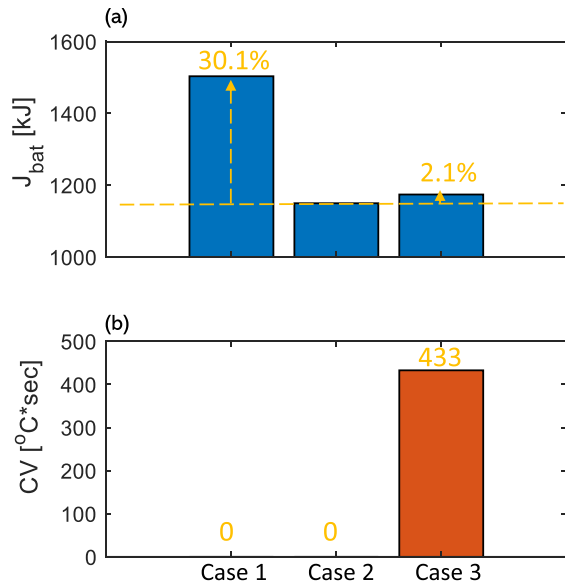


Fig. 16. Energy consumption and battery temperature CV results of Cases 1–3. (a) Energy consumption for battery cooling (J_{bat}). (b) Accumulated T_{bat} CV.

C. Location-Dependent Thermal Constraint for Improved MPC Robustness

As previously discussed in Section V-A, for the repeated commuting trip data, although the test vehicle follows the same route on different work days, the large traction power events happen at different times and locations along the route. The locations where the CV occurs are marked in Fig. 17(a). Note that we can compute the event probability and the maximum CV at each location. The event probability means the probability of the battery temperature CV when the vehicle passes through certain locations and only a short prediction horizon is used in Case I. It can be observed that there is only a finite number of locations that have a nonzero probability of CV based on historical trip data. This observation suggests

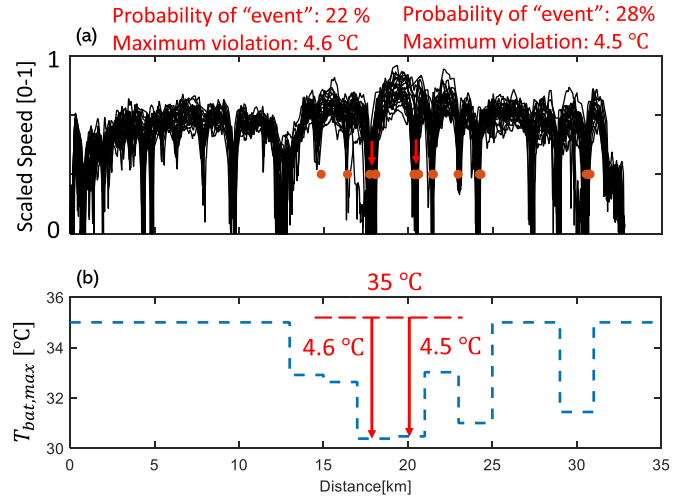


Fig. 17. (a) Aggregated vehicle speed profiles in the spatial domain. (b) Concept of the location-dependent constraint handling strategy.

a relationship between the high traction power event probability and the specific locations across the route. To leverage this relationship, a location-dependent constraint handling in MPC-based thermal management strategy is proposed and presented in Fig. 17(b).

The location-dependent constraint handling strategy tightens the upper limit of the battery temperature constraint based on the high traction power event probability and the maximum expected temperature CV. If over a certain range, there is a probability of CV based on the historical data, the upper limit, $T_{bat,max}$, is tightened based on the maximum violation of Case I. For example, two locations highlighted in Fig. 17 have a high traction power event probability of 22% and 28%, respectively, and their maximum T_{bat} violation are 4.6 °C and 4.5 °C, respectively. Therefore, the upper battery temperature limits of these two locations are tightened by 4.6 °C and 4.5 °C in the MPC formulation, once these two locations are detected within the controller prediction horizon. Whereas, for those locations where no CV was observed based on historical data, no constraint tightening will be performed, i.e., $T_{bat,max} = 35$ °C.

To demonstrate the benefits of the proposed location-dependent constraint handling strategy, a new Case 4 is defined as follows and compared against Cases 1–3.

- 1) *Case 4*: The preview information is based on the average speed shown in Fig. 14 and is subject to uncertainties. The prediction horizon length is 200 sec; the location-dependent constraint is imposed on the upper limit of the battery temperature over the trip.

The state trajectories with MPC are presented in Fig. 18, and the energy consumption and accumulated CV are summarized in Fig. 19. It can be seen from Fig. 18 that with the uncertain vehicle speed over the long horizon, the battery temperature constraints can be enforced over the entire trip thanks to the proposed location-dependent battery temperature constraint handling strategy. It demonstrates that the location-dependent constraint enhances the capacity to enforce the battery temperature constraint, resulting in improved algorithmic robustness against uncertainties in preview information.

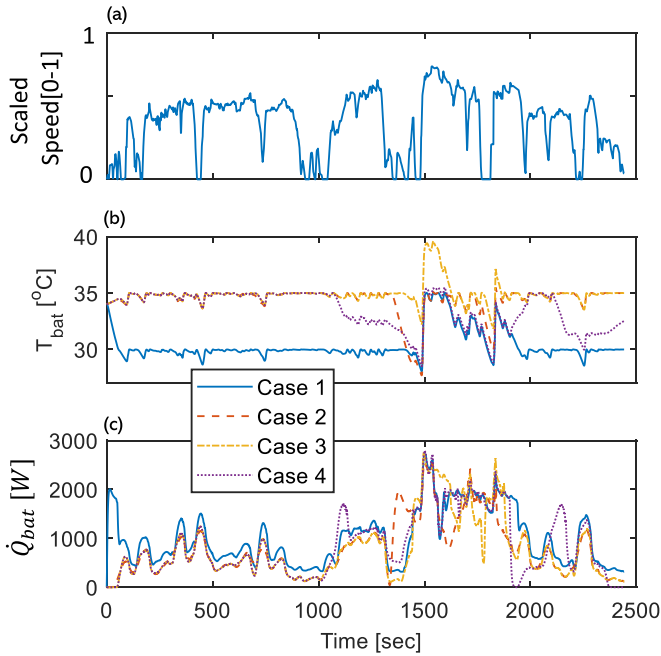


Fig. 18. State trajectories of Cases 1–4. (a) Vehicle speed. (b) Battery temperature. (c) Battery cooling power.

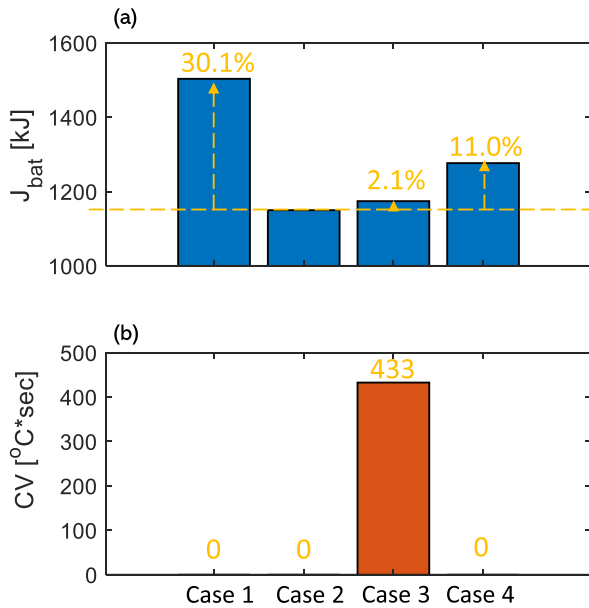


Fig. 19. Results of Cases 1–4. (a) Energy consumption for battery cooling (J_{bat}). (b) Accumulated CV.

D. Combine Location-Dependent Constraint With the Adaptive Optimization Horizon

In this section, we combine two strategies developed in this work, i.e., the location-dependent constraint and adaptive optimization horizon. A new case is defined as follows.

- 1) *Case 5*: The preview information is based on the average speed shown in Fig. 14 and is subject to uncertainties. The adaptive optimization horizon is adopted; the location-dependent constraint is imposed on the upper limit of the battery temperature over the trip.

Similar to the adaptive strategy used in Section III, the prediction horizon is set to 200 sec, and the optimization horizon

TABLE II

SIMULATION RESULTS OF CASE 4 AND 5. J_{bat} AND J_{cab} ARE THE ENERGY CONSUMPTION FOR THE BATTERY AND CABIN TMS. J_{total} IS THE TOTAL ENERGY CONSUMPTION FOR TMS

Case	4	5
J_{bat} [kJ]	1277	1278
J_{cab} [kJ]	4952	4952
J_{total} [kJ]	6229	6230
Computational Time (Average) [sec]	0.70	0.80
Constraint Violation [°C*sec]	0	0

is based on the prediction of events. As shown in Fig. 17, once the event is detected over the prediction horizon, and the upper bound of battery temperature is tightened, the optimization horizon is set to 200 sec. Otherwise, if no constraint tightening is needed over the prediction horizon, the optimization horizon is set to 50 sec to reduce the computational footprint.

As shown in Table II, the results demonstrate that both Case 4 and 5 can effectively enforce the battery temperature constraint, in the presence of an uncertain preview. Case 5, in particular, achieves similar energy consumption for both battery and cabin thermal management when compared with Case 4. This finding reaffirms that long-range optimization is only necessary when a special event is detected over the prediction horizon. Additionally, Case 5 reduces the average computational time due to its adaptive optimization horizon.

Overall, the simulation results demonstrate that by combining the two strategies developed in this article, the controller achieves a reduced computational time while enhancing its capacity to enforce battery temperature constraints with uncertain previews.

VI. CONCLUSION

EVs rely on TMS to maintain optimal battery and cabin temperatures, which consumes a significant amount of energy. To improve the efficiency of the TMS and increase the driving range of EVs, this article proposes an MPC-based strategy. Thermal systems have relatively slow dynamics, which require a long prediction horizon, making accurate forecasting of vehicle speed and traction power challenging. This article demonstrates that predicting critical events, such as the timing and magnitude of large changes in vehicle speed and traction power, can significantly improve the MPC-based TMS performance. Moreover, an adaptive strategy is developed to adjust the optimization horizon based on the observation of the critical events over the prediction horizon, which reduces the average computational time for the optimal controller. A comprehensive sensitivity analysis was conducted to evaluate the robustness of the MPC controller with respect to the uncertainties against the critical features. Furthermore, to test the MPC-based thermal management strategy, real-world drive cycles were used, and a location-dependent thermal constraint handling strategy was proposed to enhance the controller's capacity to enforce the constraints in the presence of preview uncertainties.

Future research will focus on the following aspects. First, the battery thermal model adopted in this article is simplified. The impact of the model mismatch caused by the simplification of the modeling will be investigated in future work. Second, in this study, we focus on one certain type of event, i.e., peak traction power caused by acceleration/deceleration. However, there are other events that could influence vehicle traction and thermal loads, such as road grade and door-opening events, which need to be properly considered for a better understanding of the robustness of the algorithm. Third, battery degradation will impact battery TMS, algorithms to detect and incorporate battery state of health will be developed in future work. Last, in this work, we mainly focused on battery thermal management and used a simple model to describe the cabin comfort attribute. To more accurately quantify cabin comfort, more complicated models, e.g., the predicted mean vote (PMV) model, are needed and will be studied in future work.

ACKNOWLEDGMENT

The authors would like to thank Hao Wang and Connie Qiu from Ford Motor Company, Dearborn, MI, USA, for their technical comments during the course of this study.

REFERENCES

- [1] D. Pevec, J. Babic, A. Carvalho, Y. Ghiassi-Farrokhfal, W. Ketter, and V. Podobnik, "A survey-based assessment of how existing and potential electric vehicle owners perceive range anxiety," *J. Cleaner Prod.*, vol. 276, Dec. 2020, Art. no. 122779.
- [2] C. Fiori, K. Ahn, and H. A. Rakha, "Power-based electric vehicle energy consumption model: Model development and validation," *Appl. Energy*, vol. 168, pp. 257–268, Apr. 2016.
- [3] E. E. Michaelides, "Thermodynamics and energy usage of electric vehicles," *Energy Convers. Manage.*, vol. 203, Jan. 2020, Art. no. 112246.
- [4] S. Chowdhury et al., "Total thermal management of battery electric vehicles (BEVs)," SAE Tech. Paper DOE-MAHLE-06840-1, 2018.
- [5] L. Horrein, A. Bouscayrol, W. Lhomme, and C. Dépature, "Impact of heating system on the range of an electric vehicle," *IEEE Trans. Veh. Technol.*, vol. 66, no. 6, pp. 4668–4677, Jun. 2017.
- [6] M. Jeffers, L. Chaney, and J. Rugh, "Climate control load reduction strategies for electric drive vehicles in warm weather," National Renew. Energy Lab., Golden, CO, USA, Tech. Rep. NREL/CP-5400-63551, 2015.
- [7] A. Lahlou, F. Ossart, E. Boudard, F. Roy, and M. Bakhouya, "A dynamic programming approach for thermal comfort control in electric vehicles," in *Proc. IEEE Vehicle Power Propuls. Conf. (VPPC)*, Aug. 2018, pp. 1–6.
- [8] Y. Masoudi, A. Mozaffari, and N. L. Azad, "Battery thermal management of electric vehicles: An optimal control approach," in *Proc. ASME Dyn. Syst. Control Conf.*, 2015, p. V001T13A003.
- [9] I. Cvok, B. Škugor, and J. Deur, "Control trajectory optimisation and optimal control of an electric vehicle HVAC system for favourable efficiency and thermal comfort," *Optim. Eng.*, vol. 22, no. 1, pp. 83–102, Mar. 2021.
- [10] A. Rashid, T. Hofman, and B. Rosca, "Enhanced battery thermal management systems with optimal charge control for electric vehicles," in *Proc. Annu. Amer. Control Conf. (ACC)*, Jun. 2018, pp. 1849–1854.
- [11] E. Kim, K. G. Shin, and J. Lee, "Real-time battery thermal management for electric vehicles," in *Proc. ACM/IEEE Int. Conf. Cyber-Phys. Syst. (ICCP)*, Apr. 2014, pp. 72–83.
- [12] J. van Kampen, T. Herrmann, T. Hofman, and M. Salazar, "Optimal endurance race strategies for a fully electric race car under thermal constraints," 2023, *arXiv:2301.08060*.
- [13] M. Konda, T. Hofman, and M. Salazar, "Energy-optimal design and control of electric powertrains under motor thermal constraints," in *Proc. Eur. Control Conf. (ECC)*, Jul. 2022, pp. 1178–1185.
- [14] S. Chakraborty et al., "Parameterized cloud-connected electro-thermal modelling of a battery electric vehicle," in *Proc. IEEE Vehicle Power Propuls. Conf. (VPPC)*, Oct. 2021, pp. 1–8.
- [15] A. Hamednia, N. Murgovski, J. Fredriksson, J. Forsman, M. Pourabdollah, and V. Larsson, "Optimal thermal management, charging, and eco-driving of battery electric vehicles," 2022, *arXiv:2205.01560*.
- [16] Y. Dahmane, R. Chenouard, M. Ghanes, and M. Alvarado-Ruiz, "Optimized time step for electric vehicle charging optimization considering cost and temperature," *Sustain. Energy, Grids Netw.*, vol. 26, Jun. 2021, Art. no. 100468.
- [17] A. Hamednia et al., "Optimal thermal management and charging of battery electric vehicles over long trips," 2022, *arXiv:2210.03393*.
- [18] I. Cvok, I. Ratković, and J. Deur, "Multi-objective optimisation-based design of an electric vehicle cabin heating control system for improved thermal comfort and driving range," *Energies*, vol. 14, no. 4, p. 1203, Feb. 2021.
- [19] S. Schaut and O. Sawodny, "Thermal management for the cabin of a battery electric vehicle considering passengers' comfort," *IEEE Trans. Control Syst. Technol.*, vol. 28, no. 4, pp. 1476–1492, Jul. 2020.
- [20] M. R. Amini, J. Sun, and I. Kolmanovsky, "Two-layer model predictive battery thermal and energy management optimization for connected and automated electric vehicles," in *Proc. IEEE Conf. Decis. Control (CDC)*, Dec. 2018, pp. 6976–6981.
- [21] M. R. Amini, I. Kolmanovsky, and J. Sun, "Hierarchical MPC for robust eco-cooling of connected and automated vehicles and its application to electric vehicle battery thermal management," *IEEE Trans. Control Syst. Technol.*, vol. 29, no. 1, pp. 316–328, Jan. 2021.
- [22] H. Wang, M. Amini, Z. Song, J. Sun, and I. Kolmanovsky, "Combined energy and comfort optimization of air conditioning system in connected and automated vehicles," in *Proc. Dyn. Syst. Control Conf. (DSCC)*, 2019, paper. V001T08A001, pp. 1–9.
- [23] S. Park and C. Ahn, "Computationally efficient stochastic model predictive controller for battery thermal management of electric vehicle," *IEEE Trans. Veh. Technol.*, vol. 69, no. 8, pp. 8407–8419, Jun. 2020.
- [24] M. Ebrahimi, M. Rastegar, M. Mohammadi, A. Palomino, and M. Parvania, "Stochastic charging optimization of V2G-capable PEVs: A comprehensive model for battery aging and customer service quality," *IEEE Trans. Transport. Electrific.*, vol. 6, no. 3, pp. 1026–1034, Sep. 2020.
- [25] S. Park and C. Ahn, "Model predictive control with stochastically approximated cost-to-go for battery cooling system of electric vehicles," *IEEE Trans. Veh. Technol.*, vol. 70, no. 5, pp. 4312–4323, May 2021.
- [26] M.-Y. Lee, H.-S. Lee, and H.-P. Won, "Characteristic evaluation on the cooling performance of an electrical air conditioning system using R744 for a fuel cell electric vehicle," *Energies*, vol. 5, no. 5, pp. 1371–1383, May 2012.
- [27] M. Fayazbakhsh and M. Bahrani, "Comprehensive modeling of vehicle air conditioning loads using heat balance method," SAE Tech. Paper 2013-01-1507, 2013, doi: 10.4271/2013-01-1507.
- [28] A. Pesaran, *Tools For Designing Thermal Management of Batteries in Electric Drive Vehicles*. Nat. Renew. Energy Lab., Golden, CO, USA, Tech. Rep. NREL/PR-5400-57747, 2013.
- [29] M. Risbeck and J. Rawlings. (2016). *MPCTools: Nonlinear Model Predictive Control Tools for CasADi*. [Online]. Available: <https://bitbucket.org/rawlings-group/octave-mpctools>
- [30] A. Wächter and L. T. Biegler, "On the implementation of an interior-point filter line-search algorithm for large-scale nonlinear programming," *Math. Program.*, vol. 106, no. 1, pp. 25–57, Mar. 2006.
- [31] J. A. E. Andersson, J. Gillis, G. Horn, J. B. Rawlings, and M. Diehl, "CasADi: A software framework for nonlinear optimization and optimal control," *Math. Program. Comput.*, vol. 11, no. 1, pp. 1–36, Mar. 2019.
- [32] Q. Hu et al., "A spatial data-driven vehicle speed prediction framework for energy management of HEVs using multi-horizon MPC with non-uniform sampling," in *Proc. Amer. Control Conf. (ACC)*, Jun. 2022, pp. 1024–1029.